Songklanakarin J. Sci. Technol.
43 (4), 1022-1030, Jul. - Aug. 2021

http://www.sjst.psu.ac.th

Original Article

Characterization of AA5052-ZrO_2 and AA5052-SiO_2 surface composites fabricated by friction stir processing

Mirza Abdul Hadi Baig, R. Vaira Vignesh*, R. Padmanaban, and M. Govindaraju

Department of Mechanical Engineering, Amrita School of Engineering, Coimbatore, Amrita Vishwa Vidyapeetham, India

Received: 17 August 2019; Revised: 19 February 2020; Accepted: 5 August 2020

Abstract

Friction stir processing is a surface modifying technique that allows microstructural modification and is being applied to control the behavior of a number of alloys. Surface composites of AA5052 alloy were fabricated by reinforcing zirconia (ZrO_2) and silica (SiO_2) particles by this process to improve the mechanical and corrosion properties. The developed surface composites of AA5052-ZrO_2 and AA5052-SiO_2 had a homogeneous distribution of particles with tensile strength equivalent to that of the base material. However, the hardness and corrosion behavior was different for both the composites. A significant improvement in microhardness was observed in the AA5052-ZrO_2 surface composite while AA5052-SiO_2 had microhardness similar to that of the base alloy. In the case of corrosion rate, AA5052-SiO_2 had the least among the tested specimens while AA5052-ZrO_2 showed no significant change. Fractography analysis and corrosion mechanism of the corroded specimens are also presented comprehensively.

Keywords: aluminium alloys, friction stir processing, surface composite, corrosion rate, fractography

1. Introduction

The incessant need for materials with desired properties to suit the wide engineering applications, a great deal of research work is being carried out on lightweight alloys. Aluminum alloys are specifically used in most of the engineering domain, as it has a number of advantages such as lightweight, good strength to weight ratio, non-magnetic, ductile and inexpensive. Among the different grades of aluminum alloys, AA5052 alloy is copiously used in the speedboat hulls and aircraft components. The corrosion resistance of AA5052 alloy is attributed to the presence of a surface oxide film which when damaged will result in a high corrosion rate. Hence, researchers have been working on different strategies to improve the corrosion resistance of AA5052 alloy. Compositing technology offers an extensive scope to improve corrosion resistance in AA5052 alloy among the available technologies.

*Corresponding author
Email address: r_vairavignesh@cb.amrita.edu

Composites are a new class of materials that are made by reinforcing a new phase material into the base material matrix, with an objective to obtain desirable properties. Composites in which the surface of the base material is reinforced with a constituent quantity of reinforcements are termed as surface composites. Existing techniques for the development of surface composites rely on the processing of materials at high temperatures (liquid state), which initiates an interfacial reaction between the reinforcement and matrix to form detrimental phases. This could be eliminated if the surface composites are fabricated in the solid-state (at a temperature well below the melting point of the matrix).

Solid-state processing involves subjecting the alloys to plasticization temperature and high-strain in the course of fabrication. The recovery and recrystallization phenomenon ensures desirable metallurgical, mechanical, corrosion and tribological properties. Among the solid-state processing techniques like equal channel angular pressing, accumulative roll bonding, extrusion, and rolling, less residual stress and distortion enable friction stir processing (FSP) to be widely applicable to different materials.

Friction stir processing is a new thermo-mechanical processing technique developed by Rajiv Mishra based on the concept of friction stir welding (FSW) by The Welding Institute (TWI), UK. In this technique, the workpiece is subjected to plastic deformation by a non-consumable rotating tool that is plunged into the workpiece and is made to travel in a lateral direction. This technique can also be used in the incorporation of reinforcements into the surface of the material to fabricate surface composites. The main purpose of developing this process is a microstructural modification of materials preferably in the near-surface layers (Mishra & Ma, 2005) (Węglowski, 2018). This process can be used to vary the yield strength, tensile strength, corrosion resistance, hardness and wear resistance of a material (Fuller & Mahoney, 2006)(Harikeshava, Srinivasan, & Vignesh, 2017). The most prominent processing parameters that influence friction stir processing are tool rotation speed (TRS), tool traverse speed (TTS), shoulder diameter (SD) and pin geometry. The number of passes also influences the mechanical and corrosion properties of the material (Padmanaban, Kishore, & Balusamy, 2014; Rahsepar & Jarahimoghadam, 2016).

The grain size of the stirred zone in FSP decreases with the number of passes because the strain increases with an increase in the number of passes, which in turn leads to a reduction in grain size and fine dispersion of reinforcements (Sharifitabar, Sarani, Khorshahian, & Afarani, 2011). Using micron and nanophase particles like SiC, Al_2O_3, ZrO_2, WC, TiC, B_4N, etc as reinforcements will lead to refined microstructure and reduction of grain growth. However, with just a single pass the particles will not be distributed properly. Hence, multiple passes of FSP are required to fabricate the surface composites (Bodaghi & Dehghani, 2017; Khodabakhshi, Simchi, Kokabi, Sadeghahmadi, & Gerlich, 2015). Grooves are usually made on the plates in order to properly deposit the reinforcement particles (Lim, Shibayanagi, & Gerlich, 2009; Wang, Shi, Liu, Li, & Li, 2008). Optimizing the FSP parameters will yield improved mechanical properties because of the reduction in the grain size and fragmentation of secondary phase particles (Karthikeyan, Senthilkumar, & Padmanabhan, 2010; Salehi, Saadatmand, & Aghazadeh Mohandesi, 2012). The microhardness would be considerably increased by FSP through uniform distribution of reinforcements and severe plastic deformation leading to recovery and recrystallization phenomenon (Izadi *et al.*, 2013).

As 5xxx aluminum alloys have major applications in the marine industry, the primary form of corrosion is through direct interaction with seawater. The reaction of chloride ions and the influence of FSP on the corrosion rate of 5xxx aluminum alloy was elucidated in the previous research works (Vignesh & Padmanaban, 2017).

A detailed study on the influence of zirconia and silica on the mechanical and corrosion properties of friction stir processed aluminum alloy 5052 is not available in the open literature. This study bridges the gap in the existing literature by studying how the addition of powder particles as reinforcements creates composites which may replace the existing components with a better operating life exhibiting better properties. The need for new and better composites to replace the existing conventional materials is being experienced throughout the industries. In this study, zirconia and silica powders are introduced into the aluminum alloy AA5052 matrix by using friction stir processing to improve the properties. The resulting composite could be used in the marine industry. A comprehensive analysis of the microstructure evolution, microhardness, tensile properties, fractography, corrosion properties, and corrosion mechanism is presented. A comparative analysis was presented on the developed surface composites.

2. Materials and Methodology

2.1 Materials

Aluminum alloy AA5052 sheet was chosen as the base material for this study. The composition of the alloy is as follows: 2.45% of Mg, 0.24% of Cr, 0.08% of Cu, 0.26% of Fe, 0.12% of Mn, 0.19% of Si, 0.12% of Zn, and rest Al. The sheet was cut into workpieces of dimension 150 mm x 50 mm x 5 mm using a hydraulic shear cutter. The reinforcements used were industrial-grade micron phase zirconia (ZrO_2) and nanophase silica (SiO_2). The average particle size of ZrO_2 was 50 µm and that of SiO_2 was 15 nm.

2.2 Friction stir processing

The friction stir processing trials were performed in a friction stir welding setup. High carbon high chromium steel (HCHCr) was used to fabricate the FSP tool and sealing tool. A rectangular groove of dimension 100 mm x 1 mm x 1 mm and a linear array of cylindrical holes of dimension ϕ 1mm x 1mm were machined on five workpieces each. Figure 1 shows the typical plan of grooves and hole pattern that was machined on the workpiece. The process parameters that were considered in this study were tool rotational speed (TRS), tool traverse speed (TTS), tool shoulder diameter (SD) and the number of passes. Table 1 shows the trial number and corresponding process parameters.

The workpieces were cleaned and degreased with acetone before the sealing pass. The reinforcements were filled in the groove/holes and were subjected to sealing pass using the sealing tool of shoulder diameter of 12 mm. Then FSP trials were performed on the workpieces using the FSP tool of shoulder diameter 18 mm, pin diameter of 5 mm and pin height of 3.5 mm. A dwell time of about 20 minutes was adopted between two consecutive passes.

Figure 1. Provision to fill reinforcement particles: a) Rectangular groove; b) Linear array of cylindrical holes

Table 1. Experimental layout

Sl. no	FSP trial number	FSP process parameters			
		TRS	TTS	SD	Number of passes
1	Trial01	750	20	15	1
2	Trial02	750	20	15	2
3	Trial03	750	20	18	1
4	Trial04	750	20	18	2
5	Trial05	900	10	15	1
6	Trial06	900	10	15	2
7	Trial07	900	10	18	1
8	Trial08	900	10	18	2
9	Trial09	1000	30	15	1
10	Trial10	1000	30	15	2
11	Trial11	1000	30	18	1
12	Trial12	1000	30	18	2

Based on the defect analysis of specimens optimum parameters were established for surface modification of AA5052 alloy by FSP and surface composite fabrication of AA5052 alloy by FSP. Table 2 lists the optimum level of process parameters and corresponding specimen code for surface-modified AA5052 alloy and surface composite of AA5052 alloy.

2.3 Microstructure

The BM, transverse section of the AA5052-ZrO_2 and transverse section of AA5052-SiO_2 specimens were prepared in accordance with the standard ASTM E3-11. The mirror-polished surface of the specimens was etched for 15 seconds using Poulton's reagent (HCl 60%, HNO_3 30%, HF 5% and H_2O 5%) as per standard metallographic procedures. After this, the specimen was rinsed in cold water, and then in acetone immediately. The microstructure was observed using an optical microscope (Make: Carl Zeiss).

2.4 Microhardness

Specimens *(*BM, FSP01, FSP02, AA5052-ZrO_2, and AA5052-SiO_2*)* were prepared for microhardness testing as per the directions of the standard ASTM E3-11 and were tested in a Vicker's microhardness tester (Make: Mitutoyo, Model: 201-101E). Specimens were indented at different locations using a diamond indenter at a load of 100 gf for 15 s. The diagonal length of the indents was measured and was used to calculate the microhardness. Three samples were tested in each case and their average microhardness is presented in the article.

2.5 Tensile test

Three tensile test specimens were prepared from BM, FSP01, FSP02, AA5052-ZrO_2, and AA5052-SiO_2 according to the standard ASTM E-8M-08. The dimensions of the tensile strength specimens were as follows: Gauge length of 28.57 mm, grip length of 25.04 mm, grip width of 9.525 mm, and fillet radius of 2.5 mm. Universal testing machine (Model: H25KT, Make: Tinius Olsen) was used to assess the tensile strength of the specimens at a strain rate of 0.01 per min. The maximum load capacity of the setup is 2,500 kg.

Table 2. Sample codes of the different specimens

Sl. no.	Specimen	Sample code	Process parameters
1.	Base metal AA5052	BM	
2.	Single pass friction stir processing of AA5052	FSP01	
3.	Double pass friction stir processing of AA5052	FSP02	TRS = 900 rpm
4.	Surface composite of AA5052 and ZrO_2 with friction stir processing	AA5052-ZrO_2	TTS = 10 mm/min SD = 18 mm
5.	Surface composite of AA5052 and SiO_2 with friction stir processing	AA5052-SiO_2	

Three such samples were tested for each case and their average tensile strength is presented.

2.6 Immersion corrosion test

Three sets of corrosion test specimens were cut from BM, FSP01, FSP02, AA5052-ZrO_2, and AA5052-SiO_2 and were prepared to obtain a mirror-polish surface. The dimensions of the specimen were measured using a digital vernier caliper with a least count of 0.01 mm. The specimens were weighed in a digital weighing balance with a readability of 0.0001g. Glass flasks with stoppers were filled with a 3.5% NaCl solution (simulated seawater solution). The specimen edges were rested against the walls of the glass container. The temperature of the solution was maintained at 35 °C using a thermostatic water bath. The setup was left undisturbed for 24 hours. After the immersion period, the specimens were removed from the container and were cleaned using an ultrasonicator. The average mass loss of the three samples from each case was used to calculate the corrosion rate.

2.7 Characterization using analytical instruments

Surface, chemical and phase characterizations of the specimens were carried out using Field Emission Scanning Electron Microscopy (FESEM) (Make: Zeiss Sigma), X-Ray Diffraction (XRD) (Model: Ultima 4, Make: Rigaku) and Energy Dispersive Spectroscopy (EDS) (Make: Bruker). Standard metallurgical preparation techniques were followed for preparing the specimens.

3. Results and Discussions

3.1 Defect analysis

The trial runs were carried out as per the layout given in Table 1 to achieve a defect-less FSPed zone. The defects were analyzed from macrostructure analysis. The typical defects observed in the trial specimens (Trial01 to Trial12) were root flow defects, lack of fill, pinholes, surface galling, onion ring patches and wormholes which are shown in Figure 2(e) and Figure 2(f). The formation of defects is attributed to a discordant combination of TRS, TTS, and SD. For example, high TRS or low TTS results in excessive heat input, turbulent flow of material and improper material flow

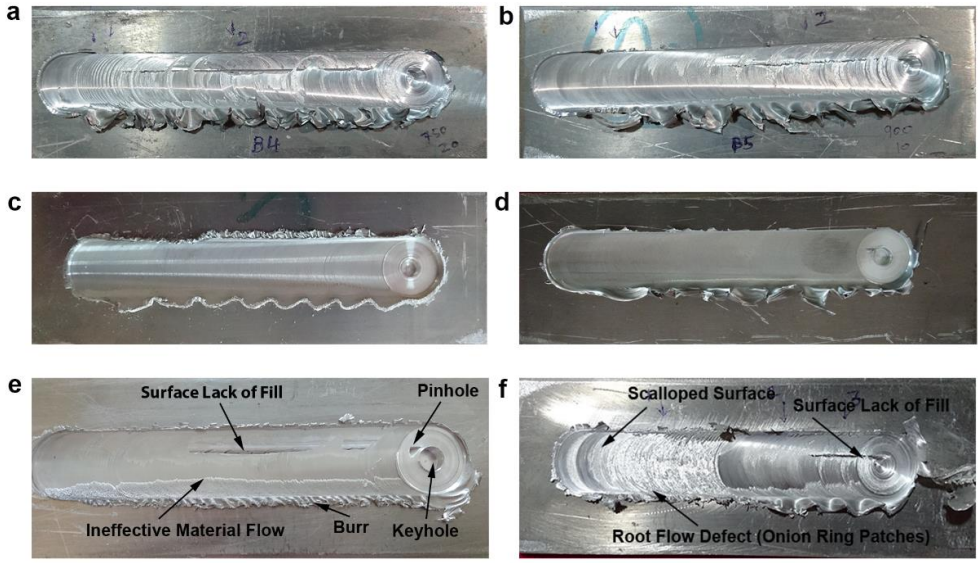

Figure 2. FSPed plates ar different process parameters: a) Trial04; b) Trial05; c) Trial10; d) Trial08; e) & f) Defects encountered in trial FSP runs.

characteristics. In the case of high TTS and low TRS, low heat input causes ineffective plasticization of material. These concepts attributed to the defects in the FSPed zone.

Figure 2 and Figure 3 presents the friction stir processed specimen's surface and macrostructure**.** Based on the microstructural analysis, the specimen Trial08 that was FSPed at TRS of 900 rpm, TTS of 10 mm/min using the FSP tool of SD of 18 mm resulted in defect-less FSPed zone**.** Hence, the parameters that were used in Trial08 were established as optimum process parameters for surface modification and surface composite fabrication in AA5052 alloy. Comparative analysis of the dispersion of reinforcements revealed that the surface composite fabricated using a rectangular groove had homogenous dispersion than that of an array of cylindrical holes**.** Hence, metallurgical, mechanical, and corrosion properties of the surface composites that were fabricated at TRS = 900 rpm, TTS = 10 mm/min, SD = 18 mm with rectangular groove for reinforcements are discussed in the following section.

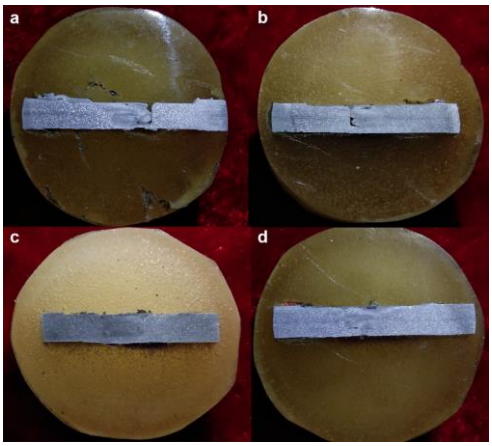

Figure 3. Macrostructures: a) Trial01; b) Trial06; c) Trial08; d) Trial12

3.2 Microstructure

Figure 4(a) shows the microstructure of the BM and Figure 4(b) shows the microstructure of the specimen FSP02**.** In Figure 4(a) and Figure 4(b), the primary phase of the alloy (α - Al) was seen as bright regions and the intermetallic phase (β - Al_2Mg_3) was seen as dark regions**.** Figure 4(c) and Figure 4(d), show the microstructure of the specimen AA5052-ZrO_2 and AA5052-SiO_2, respectively**.** The microstructural analysis confirmed the homogeneous dispersion of the β phase and reinforcement particles in the surface composites**.** Figure 5(a) and Figure 5(b) show the elemental map of the specimen AA5052-ZrO_2 and AA5052-SiO_2 respectively**.** The elemental map evidenced the homogeneous dispersion and non-agglomeration of the β phase and reinforcement particles in the surface composites**.** XRD analysis confirmed the presence of the α phase and the β phase**.** In addition, significant peaks were observed for ZrO_2 in the specimen AA5052-ZrO_2 and SiO_2 in the specimen AA5052-SiO_2**.** This concluded that the stir zone of the surface composite was rich in reinforcements**.** Figure 6(a) and Figure 6(b) show the XRD plots of the surface composite specimens.

3.3 Microhardness

Figure 6(c) compares the microhardness of the specimens. The average microhardness of the specimen BM was 67.1 Hv. The average microhardness of single pass and double pass specimens (FSP01 and FSP02) were almost similar to that of the BM specimen. However, a significant increase in hardness was observed for the specimens AA5052-ZrO_2 and AA5052-SiO_2. The maximum microhardness of the AA5052-ZrO_2 specimen was 91.6 Hv, which is ~36% higher than that of BM. The specimen AA5052-SiO_2 exhibited a maximum microhardness of 73.3 Hv that is ~9% higher than that of BM. The results indicate that the specimen AA5052-ZrO_2 had the highest microhardness among the tested specimens. The uniform distribution of ZrO_2 particles

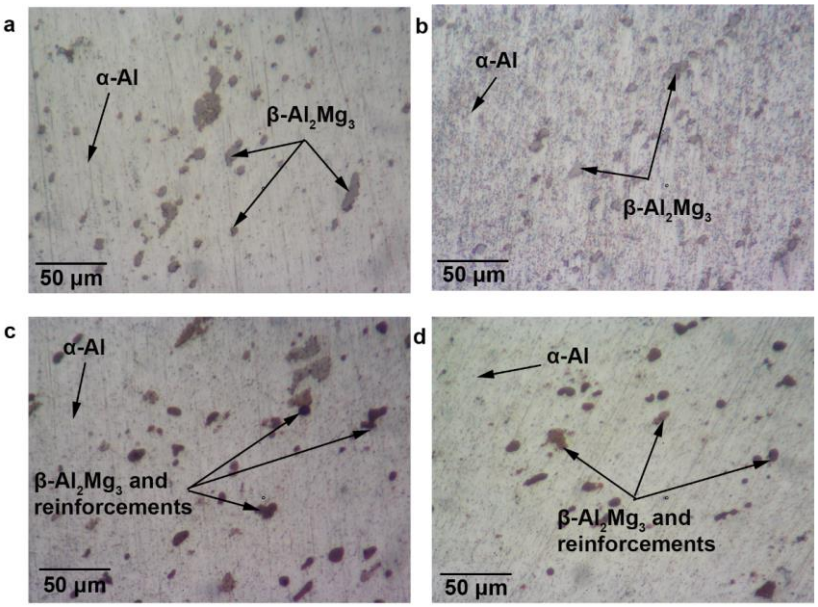

Figure 4. Microstructures: a) BM; b) FSP02; c) AA5052-ZrO_2; d) AA5052-SiO_2

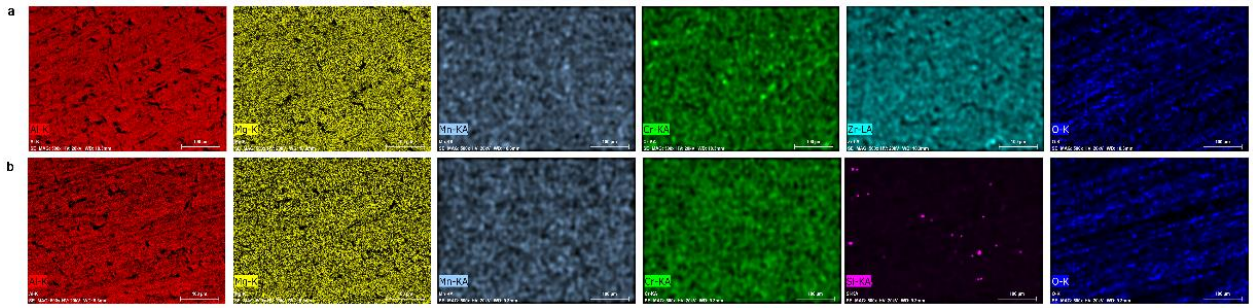

Figure 5. Elemental map a) AA5052-ZrO_2; b)AA5052-SiO_2

combined with grain refinement (induced by pinning effect of ZrO_2 and recovery and recrystallization phenomenon) was responsible for the increase in microhardness (Shahraki, Khorasani, Abdi Behnagh, Fotouhi, & Bisadi, 2013). Figure 6(d) represents the microhardness profile of the specimen AA5052-ZrO_2. It is observed that the microhardness exhibited a crest parabolic trend from the BM zone - stir zone – BM zone through thermomechanically affected zone. The lesser hardness in the thermomechanically affected zone is possibly caused by the coarsening of grains.

3.4 Tensile test

The tensile strength and % elongation of the specimens are shown in Figure 6(e) and Figure 6(f) respectively. The tensile strength of the BM was 207.44 MPa and % elongation was 22.1%. Single-pass FSP resulted in ~26% higher elongation and ~3% lower tensile strength than that of the BM. Further, FSP02 had a tensile strength of 213.55 MPa and 32% elongation that are ~4% and 45% higher than that of BM. This indicates that double pass FSP increases the tensile strength of AA5052 alloy. This increase is due to the grain refinement in the nugget zone. The strengthening could also be due to low-angle and high-angle grain boundaries (Asgharzadeh, Simchi, & Kim, 2011). In the case of AA5052-ZrO_2, the tensile strength and % elongation were 201.02 MPa and 22.33% respectively. This shows a ~3% reduction in the tensile strength and a 1% increase in elongation as compared to that of BM. The tensile strength of the specimen AA5052-SiO_2 was found to be 198.02 MPa and % elongation was 26.54%. This shows a ~4.5% reduction in the tensile strength and a ~20% increase in elongation compared with the BM. It can be noticed that the tensile properties had increased with FSP but with the addition of reinforcements, there was a reduction. The reason for this might be due to the stress buildup around the particles under tensile loading. When it reaches a critical value the matrix can no longer support the load and leads to failure (Hascalik, 2007). The tensile test results indicate that the specimen FSP02 exhibited the highest tensile strength and elongation. The %-elongation of all other specimens was higher than that of the BM specimen.

The tensile tested specimens were subjected to fractography analysis in a FESEM to deduce the fracture phenomenon. Figure 7(a)-(c) display the fractography of the specimens BM, AA5052-ZrO_2, and AA5052-SiO_2 respectively. As observed, the fractured surface in all the specimens had dimple features that were distributed all over the fractured

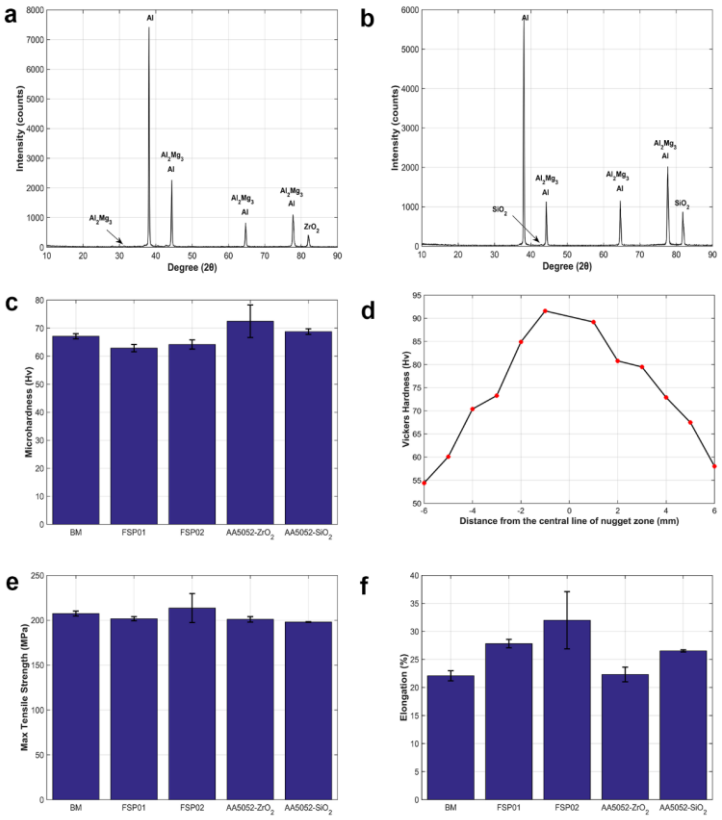

Figure 6. XRD graphs a) AA5052-ZrO_2; b) AA5052-SiO_2; c) Microhardness of base material, surface modified and surface composited specimens; d) Microhardness variation in AA5052-ZrO_2; e) Tensile Strength; f) Elongation

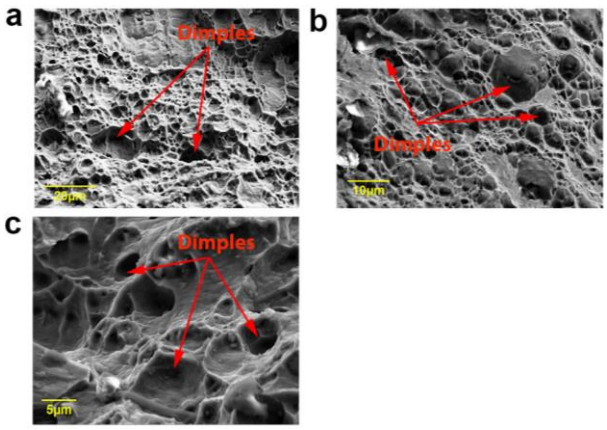

Figure 7. Fractographs: a) BM; b) AA5052-ZrO_2; c) AA5052-SiO_2

surface. This represented the plastic deformation of the specimens before failure. The nucleated crack propagates with an increase in tensile load and fails after exhibiting the yield phenomenon. A maximum ductility of 32% was measured in specimen FSP02. The addition of reinforcement particles had eventually reduced the % elongation.

3.5 Immersion corrosion test

Immersion corrosion test was done to evaluate the rate of material loss in the course of operation in the aqueous marine environment (3.5% NaCl solution). The corrosion rate was calculated using the Equation (1) based on the mass loss of the specimens after the testing period (24 hours).

$$\text{Corrosion rate} = \frac{\text{k x } \delta\text{m}}{\text{A x t x d}} \quad (1)$$

where 'k' is the conversion constant (87,600), 'δm' is the mass lost in g, 'A' is the total surface area of the specimen, 't' is the time in hours, and 'd' is the density in g/cc.

The corrosion rates of the specimens are shown in Figure 8(a). After 24 hours, the corrosion rate of the specimen BM was 0.1648 mm/year. In the case of FSP01 and FSP02, the corresponding corrosion rates were 0.6844 mm/year and 0.4808 mm/year respectively. This shows that the corrosion rate increased by ~4.16 times in FSP01 and ~2.9 times in FSP02 as compared to the corrosion rate of BM. In AA5052-ZrO_2, the corrosion rate was found to be 0.1736 mm/year; which shows an increase by only ~1.05 times that of BM. However, the corrosion rate in AA5052-SiO_2 was found to be reduced by almost 50% which was 0.0885 mm/year.

Figure 8(b) shows the surface morphology of the specimen BM after the immersion corrosion test. The specimen exhibited wide cracks and bulged surface that indicated a high corrosion rate. In addition, corrosion pits were observed on the specimen at various locations. This confirms that pitting corrosion is predominant in BM. The increased corrosion rate of specimens FSP01 and FSP02 is attributable to the coarsened β phase particles. The addition of ZrO_2 to the matrix reduced the corrosion rate as compared to

FSP01 and FSP02. However, the corrosion rate was still higher than that of the BM. In line with the increased corrosion rate, the surface morphology analysis also confirmed more deposition of corrosion products than BM, which can be noticed in Figure 8(c). The amalgamation of fine grains, dispersed β phase, and nanophase SiO_2 increased the corrosion resistance of specimen AA5052-SiO_2. Figure 8(d) shows the surface morphology of specimen AA5052-SiO_2. The fine dispersion of nanophase SiO_2 that had a higher electron work function than that of Al also contributed to the improvement in corrosion resistance. The post corrosion surface morphology analysis revealed that the specimen AA5052-SiO_2 had uniform corrosion. Besides, no characteristic pits were observed. Based on the corrosion test and surface morphology analysis, specimen AA5052-SiO_2 had better corrosion characteristics than the other tested specimens.

The corrosion mechanism of Al alloys is explained in the Equations (2)-(7). The reaction of Al with pure distilled water is shown in Equations (2)-(4).

$$Al + 3H_2O \rightarrow Al(OH)_3 + 3H^+ + 3e^- \quad (2)$$

$$Al + 2H_2O \rightarrow AlO(OH) + 3H^+ + 3e^- \quad (3)$$

$$Al + (3/2)H_2O \rightarrow Al_2O_3 + 3H^+ + 3e^- \quad (4)$$

$$Al(OH)^{2+} + Cl^- \rightarrow Al(OH)Cl^+ \quad (5)$$

$$Al(OH)Cl + H_2O \rightarrow Al(OH)_2Cl + H^+ \quad (6)$$

$$2Al(OH)_2Cl + 4Na^+ + 4Cl^- \rightarrow 2AlCl_3 + 4NaOH \quad (7)$$

Formation of $Al(OH)_3$ and Al_2O_3 on the surface reduces the corrosion rate of the specimens initially. However, $Al(OH)_3$ is highly reactive with Cl^- ions. The reaction of $AlOH_3$ with chloride ions present in the seawater further promotes the corrosion rate as given by Equations (5)-(7) (Vignesh & Padmanaban, 2017). The cracks that were formed favors diffusion of chloride ions which further increases the corrosion of the specimens. Figure 9(a) and Figure 9(b) show the elemental composition of the corroded specimens (AA5052-ZrO_2 and AA5052-SiO_2) which are in line with the above-mentioned equations.

4. Conclusions

Friction stir processing was successfully applied to AA5052 alloy to achieve surface modification and surface composites with ZrO_2 and SiO_2 reinforcements. Microstructure, microhardness, tensile and corrosion behavior of the specimens was studied. On average, the surface composites exhibited improved properties. The following observations have been derived from the study:

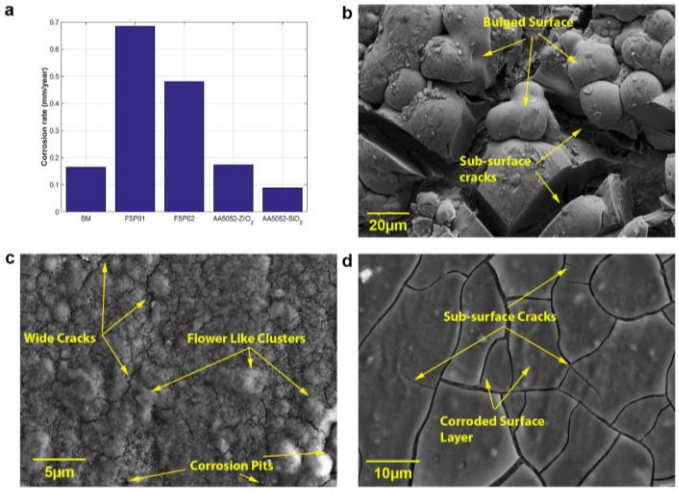

Figure 8. a) Corrosion rate; Corroded surface morphology: b) BM; c) AA5052-ZrO_2; d) AA5052-SiO_2

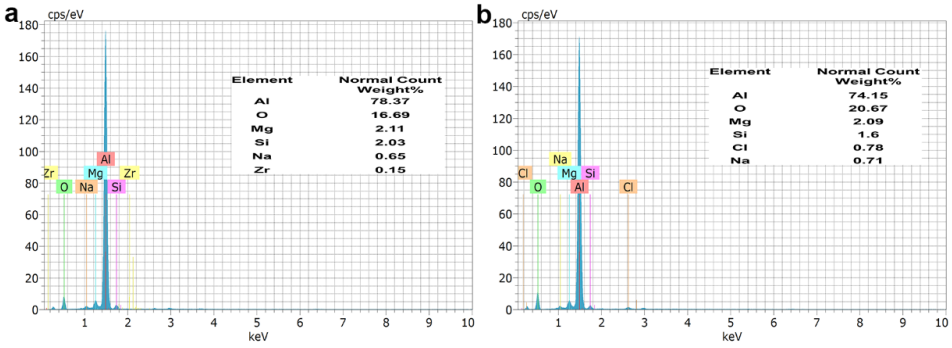

Figure 9. Elemental composition of corroded specimens a) AA5052-ZrO_2; b) AA5052-SiO_2

1. The microstructural analysis confirmed the fine grains, fragmented β phase and homogenous dispersion of reinforcements in the surface composites.

2. The maximum tensile strength (213.55 MPa), as well as the maximum % elongation (32%), was observed in FSP02 (900 rpm, 20 mm/min, double pass with shoulder diameter of 18 mm) which is ~4% and ~45% more than that of BM, respectively.

3. A maximum microhardness of 91.6 Hv was achieved in AA5052-ZrO_2 which is ~36% higher as compared to 67.1 Hv of BM.

4. Corrosion resistance improved in both the surface composites. The corrosion rate showed a significant decrease of ~50% in the specimen AA5052-SiO_2.

5. The characterization results of analytical instruments confirm that the reinforcements were uniformly dispersed in the surface composite which in turn improved the mechanical and corrosion properties. Hence, friction stir processing is a successful technique to fabricate surface composites of AA5052 alloy using ZrO_2 and SiO_2.

6. Future Scope

In the present study, only surface composites have been made based on certain applications. The work could be further applied to making composites by exploring the possibility of multi-level processing. Fatigue and creep behavior of friction stir processed materials should be studied and improved for better applications. In this study, only zirconia and silica powder particles have been incorporated in the Al alloys. Different combinations of reinforcement and alloys could be explored which might result in better composites. A mixture of reinforcement powders could also be experimented with.

References

Asgharzadeh, H., Simchi, A., & Kim, H. S. (2011). Microstructural features, texture and strengthening mechanisms of nanostructured AA6063 alloy processed by powder metallurgy. *Materials Science and Engineering A, 528*(12), 3981–3989. doi:10.1016/j.msea.2011.01.082

Bodaghi, M., & Dehghani, K. (2017). Friction stir welding of AA5052: The effects of SiC nano-particles addition. *The International Journal of Advanced Manu facturing Technology*, *88*, 2651–2660. doi:10.1007/s00170-016-8959-8

Fuller, C. B., & Mahoney, M. W. (2006). The effect of friction stir processing on 5083-H321/5356 Al arc welds: Microstructural and mechanical analysis. *Metallurgical and Materials Transactions A: Physical Metallurgy and Materials Science*, *37*(12), 3605–3615. doi:10.1007/s11661-006-1055-1

Harikeshava, R., Srinivasan, M. S., & Vignesh, R. V. (2017). Aluminium alloy AA5083. *Proceedings of the 2nd International Conference on Communication and Electronics Systems, ICCES 2017, IEEE Xplore, Volume 2018-January* (pp.716-720).

Hascalik, A. (2007). Effect of particle size on the friction welding of Al_2O_3 reinforced 6160 Al alloy composite and SAE 1020 steel. *Materials and Design, 28*(1), 313-317. doi:10.1016/j.matdes.2005.06.001

Izadi, H., Nolting, A., Munro, C., Bishop, D. P., Plucknett, K. P., & Gerlich, A. P. (2013). Friction stir processing of Al/SiC composites fabricated by powder metallurgy. *Journal of Materials Processing Technology, 213*(11), 1900-1907. doi:10.1016/j.jmatprotec.2013.05.012

Karthikeyan, L., Senthilkumar, V. S., & Padmanabhan, K. A. (2010). On the role of process variables in the friction stir processing of cast aluminum A319 alloy. *Materials and Design*, *31*(2), 761–771. doi:10.1016/j.matdes.2009.08.001

Khodabakhshi, F., Simchi, A., Kokabi, A. H., Sadeghahmadi, M., & Gerlich, A. P. (2015). Reactive friction stir processing of AA 5052 – TiO 2 nanocomposite : process – microstructure – mechanical charac teristics. *Materials Science and Technology, 31*(4), 426-435. doi:10.1179/1743284714Y.0000000573

Lim, D. K., Shibayanagi, T., & Gerlich, A. P. (2009). Synthesis of multi-walled CNT reinforced aluminium alloy composite via friction stir processing. *Materials Science and Engineering: A, 507(1-2),* 194–199. doi:10.1016/j.msea.2008.11.067

Mishra, R. S., & Ma, Z. Y. (2005). Friction stir welding and processing. *Materials Science and Engineering: R: Reports, 50*(1-2), 1–78. doi:10.1016/j.mser.2005.07.001

Padmanaban, R., Kishore, V. R., & Balusamy, V. (2014). Numerical simulation of temperature distribution and material flow during friction stir welding of dissimilar aluminum alloys. *Procedia Engineering*, *97*, 854–863. doi:10.1016/j.proeng.2014.12.360

Rahsepar, M., & Jarahimoghadam, H. (2016). The influence of multipass friction stir processing on the corrosion behavior and mechanical properties of zircon-reinforced Al metal matrix composites. *Materials Science and Engineering A, 671*, 214–220. doi:10.1016/j.msea.2016.05.056

Salehi, M., Saadatmand, M., & Aghazadeh Mohandesi, J. (2012). Optimization of process parameters for producing AA6061/SiC nanocomposites by friction stir processing. *Transactions of Nonferrous Metals Society of China (English Edition)*, *22*(5), 1055–1063. doi:10.1016/S1003-6326(11)61283-1

Shahraki, S., Khorasani, S., Abdi Behnagh, R., Fotouhi, Y., & Bisadi, H. (2013). Producing of AA5083/ZrO2 nanocomposite by friction stir processing (FSP). *Metallurgical and Materials Transactions B: Process Metallurgy and Materials Processing Science*, *44*(6), 1546–1553. doi:10.1007/s11663-013-9914-9

Sharifitabar, M., Sarani, A., Khorshahian, S., & Afarani, M. S. (2011). Fabrication of 5052Al / Al2O3 nanoceramic particle reinforced composite via friction stir processing route. *Materials and Design*, *32*(8–9), 4164–4172. doi:10.1016/j.matdes.2011.04.048

Vignesh, V., & Padmanaban, R. (2017). Modelling corrosion behavior of friction stir processed aluminium alloy 5083 using polynomial: Radial basis function. *Transactions of the Indian Institute of Metals*. doi:10.1007/s12666-017-1110-1

Wang, W., Shi, Q., Liu, P., Li, H., & Li, T. (2008). A novel way to produce bulk SiCp reinforced aluminum metal matrix composites by friction stir processing. *Journal of Materials Processing Technology, 209*(4), 2099–2103. doi:10.1016/j.jmatprotec.2008.05.001

Węglowski, M. S. (2018). Friction stir processing – State of the art. *Archives of Civil and Mechanical Engineering*, *18*(1), 114–129. doi:10.1016/j.acme.2017.06.002